A Ring Model for Understanding How Interfacial Interaction Dictates the Structures of Protection Motifs and Gold Cores in Thiolate-Protected Gold Nanoclusters

Wen Xu (xuwenwu@nbu.edu.cn)
Ningbo University https://orcid.org/0000-0002-0651-9562
Mengke Zheng
Ningbo University
Wenhua Han
Ningbo University
Pengye Liu
Ningbo University
Xiao Cheng Zeng
University of Nebraska-Lincoln https://orcid.org/0000-0003-4672-8585

Article

Keywords: thiolate-protected gold nanoclusters, ring model, interfacial interaction

Posted Date: August 7th, 2020

DOI: https://doi.org/10.21203/rs.3.rs-39976/v1

Abstract

Understanding the role of interfacial interactions between the protection motifs $SR[Au(SR)]_x$ (x = 0, 1, 2, 3, ...) and gold cores on the stabilities of the thiolate-protected gold nanoclusters is still a challenging task. Although several theoretical models, including the superatom complex, super valence bond, and superatom network, have provided insights into the stabilities of either the overall structures or the gold cores, a model that can illuminate how the interfacial interaction dictates the unique structures of the protection motifs and gold cores is still lacking. Herein, we present a ring model, on the basis of comprehensive analyses of all 95 previous experimentally crystallized and theoretically predicted thiolate-protected gold nanoclusters, to offer a deeper insight into the structure-interaction relationship for this class of clusters. In the ring model, all the thiolate-protected gold nanoclusters can be generically viewed as fusion or interlocking of several $[Au_m(SR)_n]$ (m = 4 - 8, 10, 12, and $0 \leq n \leq m$) rings. The aurophilic interactions among these rings are expected to play a key role in the stabilization of the thiolate-protected gold nanoclusters. Guided by the ring model and the grand unified model (for understanding the structures of gold cores), a new $Au_{42}(SR)_{26}$ isomer is predicted, whose total energy is even lower than those of two previously crystallized isomers, thereby giving credence to the predictability of the ring model. The ring model provides not only a mechanistic understanding of the interactions between the protection ligands and gold cores in the thiolate-protected gold nanoclusters, but also a practical guidance on predicting new thiolate-protected gold nanoclusters for experimental synthesis and confirmation.

Introduction

The chemical and structural properties of thiolate-protected gold nanoclusters that entail strong gold-sulfur (Au-S) covalent bond have received considerable attention over the past fifteen years.[1] Since the report of the first total crystalline structure of thiolate-protected gold nanocluster Au_{102}(p-MBA)$_{44}$ (p-MBA = p-mercaptobenzoic acid) in 2007,[2] the studies on the structures of thiolate-protected gold nanoclusters both through experimental crystallization and theoretical predictions have increased dramatically.[3-7] A common structural feature of the thiolate-protected gold nanoclusters is that each cluster is composed of a gold core and a number of oligomeric $SR[Au(SR)]_x$ (x = 0, 1, 2, 3, ...) protection motifs, all exhibiting core-shell interfacial structure.[3,7,8] Several theoretical models, such as superatom complex (SAC) model,[9] super valence bond (SVB) model,[10] superatom network (SAN) model,[11,12] borromean ring model,[13] grand unified model (GUM),[14-16] and thermodynamic stability theory (TST),[17] have been proposed to elucidate various properties of these core-shell clusters. For example, SAC was developed to describe the electronic structures of the thiolate-protected gold nanoclusters. SVB, SAN, and GUM were to describe generic properties of the gold cores. Borromean ring model can illuminate the structure of the prototype cluster, $Au_{25}(SR)_{18}^-$,[18-20] whose six $SR[Au(SR)]_2$ protection motifs and the icosahedral Au_{13} core are closely linked through Borromean rings. However, it is difficult to generalize the Borromean ring model to other thiolate-

protected gold nanoclusters. In the TST model, a fine energy balance between the core cohesive energy and the shell-to-core binding energy was identified. Despite of major progresses in the development of various models to understand the stabilities of either the overall structures or the gold cores, a model that can elucidate how the interfacial interaction dictates the unique structures of the protection motifs and gold cores is still lacking, which hinders the tractable design of the thiolate-protected gold nanoclusters.

In this communication, we present development of a ring model, on the basis of comprehensive analyses of all previous experimentally crystallized and theoretically predicted thiolate-protected gold nanoclusters, to offer a deeper insight into the structure-interaction relationship for these nanoclusters. We show that the nanoclusters can be decomposed into several fused or interlocked rings, namely, $[Au_m(SR)_n]$ (m = 4 - 8, 10, 12, and $0 \leq n \leq m$). These $[Au_m(SR)_n]$ rings entail aurophilic interactions that play a key role to stabilize the thiolate-protected gold nanoclusters. Furthermore, guided by the ring model and the previously developed GUM, a new $Au_{42}(SR)_{26}$ isomer is predicted to have lower energy than two crystallized isomers previously synthesized in the laboratory.

Results

Ring model: $[Au_m(SR)_n]$ (m = 4 - 8, 10, 12, and $0 \leq n \leq m$) rings.

Development of the ring model is based on detailed analysis of structures of all 95 thiolate-protected gold nanoclusters, and their atomistic structures were either determined from previous experiments (totally 41 crystallized structures) or predicted from density-functional theory (DFT) computation (totally 54 structures) over the past fifteen years. Several types of ring structures, i.e. $[Au_m(SR)_n]$ (m = 4 - 8, 10, 12, and $0 \leq n \leq m$), have been identified, as shown in Figures 1-6. In addition, the number of gold atoms in the gold core ($N_{Au\text{-}core}$), the number of elementary blocks (N_{eb}) that the gold-core atoms belong to, the number of gold atoms in the protection motifs (N_{Au}), and the number of sulfur atoms in the protection motifs (N_S) are listed in Table 1. Note that in our previously developed GUM, the gold core of ligand-protected gold nanocluster can be viewed as several elementary blocks (triangular Au_3 and tetrahedral Au_4, both satisfying duet rule) fused or packing together.[14-16]

Table 1 The number of gold core atoms ($N_{Au\text{-}core}$), the elementary blocks (N_{eb}) that the gold-core atoms belong to, the number of gold atoms in the protection motifs (N_{Au}), and the number of S atoms in the protection motifs (N_S) in $[Au_m(SR)_n]$ (m = 4 - 8, 10, 12, and $0 \leq n \leq m$) rings. For every ring class, two equations to describe the relationship among $N_{Au\text{-}core}$, N_{eb}, N_{Au}, and N_S are also presented. The

superscripts, 1a and 1b, in the table denote the corresponding ring structures shown in Figure 1a and Figure 1b, respectively.

Ring Class	Specific Rings	$N_{Au\text{-}core}$	N_{eb}	N_{Au}	N_S	Protection Motifs	Equations
$[Au_4(SR)_n]$ ($1 < n \leq 4$)	$[Au_4(\mu_3\text{-}S)_2(SR)_2]$[1a]	0	0	4	4	$[Au_4(\mu_3\text{-}S)_2(SR)_2]$ ring	$N_{Au} = 4 - N_{Au\text{-}core}$ $N_S = 4 - N_{eb}$
	$[Au_4(SR)_3]$[1b]	2	1	2	3	$SR[Au(SR)]_2$	
	$[Au_4(SR)_2]$[1c]	3	2	1	2	SR[Au(SR)]	
	$[Au_4(SR)_2]$[1d]	4	2	0	2	2SR	
$[Au_5(SR)_n]$ ($1 \leq n < 5$)	$[Au_5(SR)_4]$[2a]	2	1	3	4	$SR[Au(SR)]_3$	$N_{Au} = 5 - N_{Au\text{-}core}$ $N_S = 5 - N_{eb}$
	$[Au_5(SR)_3]$[2b,2c]	4	2	1	3	SR + SR[Au(SR)]	
	$[Au_5(SR)_2]$[2d]	4	3	1	2	SR[Au(SR)]	
	$[Au_5(SR)]$[2e]	5	4	0	1	SR	
$[Au_6(SR)_n]$ ($0 \leq n \leq 6$)	$[Au_6(SR)_6]$[3a]	0	0	6	6	$[Au_6(SR)_6]$ ring	$N_{Au} = 6 - N_{Au\text{-}core}$ $N_S = 6 - N_{eb}$
	$[Au_6(SR)_5]$[3b]	2	1	4	5	$SR[Au(SR)]_4$	
	$[Au_6(SR)_4]$[3c]	3	2	3	4	$SR[Au(SR)]_3$	
	$[Au_6(SR)_4]$[3d]	4	2	2	4	2SR[Au(SR)]	
	$[Au_6(SR)_3]$[3e]	5	3	1	3	SR + SR[Au(SR)]	
	$[Au_6(SR)_3]$[3f]	4	3	2	3	$SR[Au(SR)]_2$	
	$[Au_6(SR)_3]$[3g]	6	3	0	3	3SR	
	$[Au_6(SR)_2]$[3h]	5	4	1	2	SR[Au(SR)]	
	$[Au_6(SR)_2]$[3i]	6	4	0	2	2SR	
	$[Au_6(SR)]$[3j]	6	5	0	1	SR	
	$[Au_6]$[3k]	6	6	0	0	-	
$[Au_7(SR)_n]$ ($n = 4$ or 5)	$[Au_7(SR)_5]$[4a]	4	2	3	5	$SR[Au(SR)] + SR[Au(SR)]_2$	$N_{Au} = 7 - N_{Au\text{-}core}$

	$[Au_7(SR)_4]^{4b}$	5	3	2	4	SR + SR[Au(SR)]$_2$	$N_S = 7 - N_{eb}$
	$[Au_7(SR)_4]^{4c}$	5	3	2	4	2SR[Au(SR)]	
$[Au_8(SR)_n]$ (n = 4, 6, or 8)	$[Au_8(SR)_8]^{5a}$	0	0	8	8	$[Au_8(SR)_8]$ ring	$N_{Au} = 8 - N_{Au\text{-}core}$ $N_S = 8 - N_{eb}$
	$[Au_8(\mu_3\text{-}S)_2(SR)_4]^{5b}$	4	2	4	6	SR + SR[Au(μ_3-S)Au(SR)]$_2$	
	$[Au_8(SR)_4]^{5c}$	6	4	2	4	2SR[Au(SR)]	
$[Au_{10}(SR)_n]$ (n = 4)	$[Au_{10}(SR)_4]^{5d}$	8	6	2	4	2SR[Au(SR)]	$N_{Au} = 10 - N_{Au\text{-}core}$ $N_S = 10 - N_{eb}$
$[Au_{12}(SR)_n]$ (n = 4)	$[Au_{12}(SR)_4]^{5e}$	10	8	2	4	2SR[Au(SR)]	$N_{Au} = 12 - N_{Au\text{-}core}$ $N_S = 12 - N_{eb}$

1. $[Au_4(SR)_n]$ ($1 < n \leq 4$) rings.

As shown in Figure 1, four types of $[Au_4(SR)_n]$ ($1 < n \leq 4$) rings are identified. Except two R ligands, the $[Au_4(\mu_3\text{-}S)_2(SR)_2]$ ring structure (Figure 1a) observed in the thiolate-protected gold nanocluster $Au_{38}(\mu_3\text{-}S)_2(SR)_{20}$ is the same as $[Au_4(SR)_4]$ ring,[21] either detected experimentally as an isolated form or observed within the $[Au_8(SR)_8]$ ring to form an $Au_{12}(SR)_{12}$ structure (Figure S1).[22,23] The $[Au_4(SR)_3]$ ring seen in $Au_{21}(SR)_{15}$ (Figure 1b) can be formed by binding a SR[Au(SR)]$_2$ protection motif ($N_{Au} = 2$ and $N_S = 3$) with two gold atoms in a tetrahedron Au_4 elementary block ($N_{Au\text{-}core} = 2$ and $N_{eb} = 1$).[24] The $[Au_4(SR)_2]$ ring seen in $Au_{20}(SR)_{16}$ (Figure 1c) is formed by binding a SR[Au(SR)] protection motif ($N_{Au} = 1$ and $N_S = 2$) with two gold atoms at the two ends of the bi-tetrahedron Au_7 structure.[25] So, three gold-core atoms belong to the two tetrahedral Au_4 elementary blocks ($N_{Au\text{-}core} = 3$ and $N_{eb} = 2$). While the $[Au_4(SR)_2]$ ring seen in $Au_{38}(\mu_3\text{-}S)_2(SR)_{20}$ (Figure 1d) can be viewed as binding two SR motifs ($N_{Au} = 0$ and $N_S = 2$) with four gold-core atoms in two triangular Au_3 elementary blocks ($N_{Au\text{-}core} = 4$ and $N_{eb} = 2$).[21] So, the values of $N_{Au\text{-}core}$, N_{eb}, N_{Au}, and N_S in $[Au_4(SR)_n]$ rings satisfy the two equations $N_{Au} = 4 - N_{Au\text{-}core}$ and $N_S = 4 - N_{eb}$ (see Table 1). In addition, the structures of $[Au_4(\mu_3\text{-}S)_2(SR)_2]$ (Figure 1a) and $[Au_4(SR)_2]$ (Figure 1d) rings in the $Au_{38}(\mu_3\text{-}S)_2(SR)_{20}$ cluster indicate a structural transformation from $[Au_4(SR)_2]$ ring (Figure 1d) to $[Au_4(\mu_3\text{-}S)_2(SR)_2]$ ring (Figure 1a), which can be achieved by adding two three-coordinated μ_3-sulfido

(μ_3-S) atoms onto the two triangular Au_3 elementary blocks that are bound with the $[Au_4(SR)_2]$ ring (Figure 1d)

2. $[Au_5(SR)_n]$ ($1 \leq n < 5$) rings.

In Figure 2, the $[Au_5(SR)_4]$, $[Au_5(SR)_3]$, $[Au_5(SR)_2]$, and $[Au_5(SR)]$ rings are identified from the crystallized $Au_{16}(SR)_{12}$,[26] $Au_{30}(SR)_{18}$,[27] $Au_{43}(SR)_{25}$,[28] and $Au_{38}(\mu_3\text{-}S)_2(SR)_{20}$ clusters.[21] The $[Au_5(SR)_4]$ ring in Figure 2a is formed by combing a $SR[Au(SR)]_3$ protection motif ($N_{Au} = 3$ and $N_S = 4$) with two gold-core atoms belonging to a triangular Au_3 elementary block ($N_{Au\text{-}core} = 2$ and $N_{eb} = 1$). The $[Au_5(SR)_3]$ ring in Figure 2b can be generated by combining one SR[Au(SR)] and one SR ($N_{Au} = 1$ and $N_S = 3$) with four gold-core atoms belonging to two triangular Au_3 elementary blocks ($N_{Au\text{-}core} = 4$ and $N_{eb} = 2$). The $[Au_5(SR)_2]$ ring in Figure 2c is formed by combining a SR[Au(SR)] protection motif ($N_{Au} = 1$ and $N_S = 2$) with four gold-core atoms belonging to three tetrahedral Au_4 elementary blocks ($N_{Au\text{-}core} = 4$ and $N_{eb} = 3$). While the $[Au_5(SR)]$ ring in Figure 2d is formed by combining a SR protection motif ($N_{Au} = 0$ and $N_S = 1$) with five gold-core atoms belonging to four tetrahedral Au_4 elementary blocks ($N_{Au\text{-}core} = 5$ and $N_{eb} = 4$). Thus, the values of $N_{Au\text{-}core}$, N_{eb}, N_{Au}, and N_S in $[Au_5(SR)_n]$ ($1 \leq n < 5$) rings satisfy two equations $N_{Au} = 5 - N_{Au\text{-}core}$ and $N_S = 5 - N_{eb}$ (see Table 1). Note that the interlocked structures containing $[Au_5(SR)_n]$ rings have not been found in the crystallized thiolate-protected gold nanoclusters. Although a theoretical structure $Au_{24}(SR)_{20}$ was proposed to contain the interlocked $[Au_5(SR)_4]$ and $[Au_7(SR)_6]$ rings (Figure S2),[29] it has not been confirmed by experiment yet. Moreover, the $[Au_5(SR)_5]$ ring has not been found in any thiolate-protected gold nanoclusters yet, however, the $Au_{10}(SR)_{10}$ complex with two $[Au_5(SR)_5]$ interlocked rings has been seen in both experiment and simulations (Figure S3).[30]

Furthermore, in thiolate-protected gold nanoclusters with face-centered cubic (FCC) cores,[26-28] the $[Au_5(SR)_n]$ ring is always located on the top of a tetrahedron Au_4 elementary block, in which a special gold atom (highlighted by a red circle in the tetrahedral Au_4 elementary block) near the $[Au_5(SR)_n]$ ring does not bind with the SR motif, as shown in Figure 2a-2d. The average bond length between this special gold atom and the gold atoms in the $[Au_5(SR)_n]$ rings is 2.84 Å, indicating strong interactions between them. Hence, the $[Au_5(SR)_n]$ ring can be viewed as a protection motif, covering this special gold atom so that it does not need to bind with an extra SR motif. For $Au_{38}(\mu_3\text{-}S)_2(SR)_{20}$ with a body-centered cubic (BCC) core,[21] however, this special gold atom near the $[Au_5(SR)]$ ring no longer exists (Figure 2e) due to the gold core with different symmetry.

3. $[Au_6(SR)_n]$ ($0 \leq n \leq 6$) rings.

In Figure 3a-k, the $[Au_6(SR)_6]$ ring in $Au_{22}(SR)_{18}$,[31] $[Au_6(SR)_5]$ ring in $Au_{21}(SR)_{15}$,[32] $[Au_6(SR)_4]$ ring in $Au_{28}(SR)_{20}$ and $Au_{23}(SR)_{16}^-$ clusters,[33,34] $[Au_6(SR)_3]$ ring in $Au_{30}(SR)_{18}$,$Au_{36}(SR)_{24}$,[27,35] and $Au_{68}(SR)_{36}$

clusters,[36] $[Au_6(SR)_2]$ ring in $Au_{34}(SR)_{22}$ and $Au_{92}(SR)_{44}$ clusters,[37,38] $[Au_6(SR)]$ ring in $Au_{92}(SR)_{44}$ cluster,[38] and $[Au_6]$ ring in $Au_{40}(SR)_{24}$ cluster are presented.[39] Among them, only the $[Au_6(SR)_6]$ ring in $Au_{22}(SR)_{18}$ (Figure 3a) and the $[Au_6(SR)_3]$ ring in $Au_{68}(SR)_{36}$ (Figure 3g) have not been observed in the crystallized nanoclusters. The compositions of $[Au_6(SR)_n]$ ($0 \leq n \leq 6$) rings are also analyzed in Table 1, in which the values of $N_{Au\text{-}core}$, N_{eb}, N_{Au}, and N_S in the $[Au_6(SR)_n]$ ($0 \leq n \leq 6$) rings also satisfy two equations $N_{Au} = 6 - N_{Au\text{-}core}$ and $N_S = 6 - N_{eb}$. Moreover, the same number of gold and sulfur atoms but completely different compositions can be seen in the $[Au_6(SR)_4]$ rings (Figure 3c and 3d), $[Au_6(SR)_3]$ rings (Figure 3e, 3f, and 3g), and $[Au_6(SR)_2]$ rings (Figure 3h and 3i). Unlike the $[Au_4(SR)_n]$ ($1 < n \leq 4$) and $[Au_5(SR)_n]$ ($1 \leq n < 5$) rings, the $[Au_6(SR)_n]$ ($0 \leq n \leq 6$) rings tend to adopt the interlocked ring structures with one Au atom being located at the center of the ring (Figure S4), very similar with the $Au_{12}(SR)_{12}$ composed of two $[Au_6(SR)_6]$ interlocked rings (Figure S5).[30]

4. $[Au_7(SR)_n]$ ($2 < n < 5$) ring.

In Figure 4a, the $[Au_7(SR)_5]$ ring can be identified in $Au_{38}(SR)_{24}$ nanocluster by combining one SR[Au(SR)] and one $SR[Au(SR)]_2$ ($N_{Au} = 3$ and $N_S = 5$) with four gold-core atoms belonging to two tetrahedral Au_4 elementary blocks ($N_{Au\text{-}core} = 4$ and $N_{eb} = 2$).[40] In Figure 4b and 4c, two types of $[Au_7(SR)_4]$ rings, both found in crystallized $Au_{43}(SR)_{25}$ nanocluster,[28] can be formed, respectively, by combining one $SR[Au(SR)]_2$ and one SR ($N_{Au} = 2$ and $N_S = 4$) with five gold-core atoms belonging to two tetrahedral Au_4 and one triangular Au_3 elementary blocks ($N_{Au\text{-}core} = 5$ and $N_{eb} = 3$), and by combining two SR[Au(SR)] ($N_{Au} = 2$ and $N_S = 4$) with five gold-core atoms belonging to three tetrahedral Au_4 elementary blocks ($N_{Au\text{-}core} = 5$ and $N_{eb} = 3$). Thus, the values of $N_{Au\text{-}core}$, N_{eb}, N_{Au}, and N_S in $[Au_7(SR)_n]$ rings satisfy two equations $N_{Au} = 7 - N_{Au\text{-}core}$ and $N_S = 7 - N_{eb}$. It should be noted that one half of the $[Au_7(SR)_4]$ ring bypasses the middle of the bi-tetrahedron Au_7 structure and the other half bypasses an end of Au_7, while the whole $[Au_6(SR)_3]$ ring tends to bypass the middle of the bi-tetrahedron Au_7 structure (Figure S6). This difference can be attributed to difference in the arrangement of one gold-core atom in the two rings. In addition, the $[Au_7(SR)_4]$ ring tends to interlock with another two rings (Figure S7), different from the two interlocked $[Au_6(SR)_n]$ rings.

5. Other larger rings including $[Au_8(SR)_n]$ (n = 4 and 8), $[Au_{10}(SR)_4]$, and $[Au_{12}(SR)_4]$.

In Figure 5, three larger rings, i.e. the $[Au_8(SR)_8]$ ring in $Au_{20}(SR)_{16}$ cluster,[25] $[Au_8(\mu_3\text{-}S)_2(SR)_4]$ ring in $Au_{38}(\mu_3\text{-}S)_2(SR)_{20}$ cluster,[21] $[Au_8(SR)_4]$ ring in $Au_{28}(SR)_{20}$ cluster,[41] $[Au_{10}(SR)_4]$ ring in $Au_{72}(SR)_{40}$ cluster,[42] and $[Au_{12}(SR)_4]$ ring in $Au_{92}(SR)_{44}$ cluster,[38] are identified. Among them, the $[Au_{10}(SR)_4]$ ring has

not been confirmed by experiment yet. The $[Au_8(SR)_8]$ ring can be seen in both thiolate-protected gold nanocluster $Au_{20}(SR)_{16}$ and Au(I)-S complex $Au_{12}(SR)_{12}$ (Figure S8).[25,30] As listed in Table 1, the compositions of each ring in Figure 5 also satisfy two equations. In addition, the $[Au_8(SR)_4]$, $[Au_{10}(SR)_4]$, and $[Au_{12}(SR)_4]$ rings tend to interlock with another 2, 3, and 4 rings, respectively.

Discussion Of The Ring Model

1. The stabilities of $[Au_m(SR)_n]$ rings.

In most of $[Au_m(SR)_n]$ rings, the number of sulfur atoms is less than the number of gold atoms. In isolated forms, these independent rings are unstable, contrary to the high stabilities of the elementary blocks in the gold cores (as described by GUM).[14-16] Although the structural decompositions of thiolate-protected gold nanoclusters into $[Au_m(SR)_n]$ rings are not reflective of the electronic structure, the ring model can be still helpful to understand the interfacial interactions between $SR[Au(SR)]_x$ (x = 0, 1, 2, 3, ...) protection motifs and gold cores. Notably, the insufficient number of sulfur atoms in $[Au_m(SR)_n]$ rings can actually be offset by the growth of the μ_3-S onto the triangular Au_3 to form the $Au_3(\mu_3\text{-S})$ units or by the growth of the four-coordinated μ_4-sulfido (μ_4-S) into the tetrahedral Au_4 to form the $Au_4(\mu_4\text{-S})$ units. As shown in our recent work,[43] the structural transformation from thiolate-protected nanoclusters to more stable Au(I)-S complexes can be achieved by gradually adding the μ_3-S and/or μ_4-S motifs to the gold core. Among these predicted complexes, the number of sulfur atoms eventually becomes balanced, namely, there are the same number (6) of gold atoms as the sulfur atoms in each $[Au_6S_q(SR)_{6-q}]$ ring (integer q is the number of μ_3-S and μ_4-S atoms). Therefore, with the increment of the number of μ_3-S and μ_4-S atoms, the transformation from the unstable $[Au_m(SR)_n]$ rings associated with the thiolate-protected nanoclusters to the stable $[Au_m(SR)_m]$ rings associated with the Au(I)-S complexes can be achieved.

2. The atomic structures at the center of rings.

With the increment of the radii of rings, the atomic structures at the center of rings become increasingly complex, as shown in Figure 6. No extra gold atoms at or near the center of the smallest $[Au_4(SR)_3]$ ring can be seen (Figure 6a). For the $[Au_5(SR)_3]$ ring with a larger radius, there is one gold atom below the center of the ring (Figure 6b), and the average bond length between the gold atom and the gold atoms in the $[Au_5(SR)_3]$ rings is 2.84 Å. While for the $[Au_6(SR)_n]$ ring, one gold atom (Figure 6c) or a triangular Au_3 (Figure 6d) located at the center of ring can be found. With further increase of the radii of the rings, there are one, two, three and, four tetrahedral Au_4 structures observed in the $[Au_7(SR)_4]$, $[Au_8(SR)_8]$, $[Au_{10}(SR)_4]$, and $[Au_{12}(SR)_4]$ rings, respectively (Figure 6e-h). The same trend can also be observed in other rings.

3. Non-ring structures associated with thiolate-protected gold nanoclusters.

Besides the $[Au_m(SR)_n]$ rings associated with the thiolate-protected gold nanoclusters, there are protection motifs that do not exhibit the ring structures. For example, a $SR[Au(SR)]_2$ motif should bind with the Au(111) facet in $Au_{36}(SR)_{24}$ or with the Au(100) facet in $Au_{42}(SR)_{26}$,[35,44] as shown in Figure 7a and 7b. For the fused tetrahedron Au_6 core with an Au-Au edge in $Au_{42}(SR)_{26}$,[44] a SR[Au(SR)] motif is needed to bind with two surface gold atoms (Figure 7c). These bonding modes between the protection motifs and the gold core, as shown in Figure 7, are very common in the thiolate-protected gold nanoclusters, which can be classified as a supplemental information to understand the interfacial interactions between non-ring $SR[Au(SR)]_x$ (x = 0, 1, 2, 3, ...) protection motifs and gold cores.

Applications of $[Au_m(SR)_n]$ (m = 4 - 8, 10, 12, and $0 \leq n \leq m$) ring model

1. Structural decompositions.

According to the ring model, the complete structures of 95 thiolate-protected gold clusters can be decomposed into several $[Au_m(SR)_n]$ (m = 4 - 8, 10, 12, and $0 \leq n \leq m$) rings that can be fused, or packed, or interlocked together. Most of the crystallized and predicted structures up to date belong to this family of nanoclusters. Two distinct structural decompositions of the crystallized $Au_{24}(SR)_{20}$ and $Au_{40}(SR)_{24}$ clusters are depicted in Figures 8 and 9 as examples,[39,45] while decompositions of other clusters are plotted in the Supporting Information.

As shown in Figure 8, the $Au_{24}(SR)_{20}$ cluster is decomposed into two $Au_{12}(SR)_{10}$, fused together by sharing two gold atoms. Here, some Au-Au bonds of the Au_8 core are broken intentionally for clarity. Next, the $Au_{12}(SR)_{10}$ can be further decomposed into two interlocked $[Au_6(SR)_5]$ rings. Thus, the structure of $Au_{24}(SR)_{20}$ can be viewed as four $[Au_6(SR)_5]$ rings, fused or interlocked together. The larger $Au_{40}(SR)_{24}$ cluster can be decomposed into two interlocked structures $Au_{24}(SR)_{12}$ and $Au_{16}(SR)_{12}$ (Figure 9a). Next, the $Au_{24}(SR)_{12}$ can be viewed as one $[Au_6]$ ring and six $[Au_6(SR)_5]$ rings fused together by sharing three gold atoms (Figure 9b), while the $Au_{16}(SR)_{12}$ can be viewed as three $[Au_6(SR)_4]$ rings fused together by sharing a gold atom (Figure 9c). So, the structure of $Au_{40}(SR)_{24}$ can be viewed as three $[Au_6(SR)_4]$, one $[Au_6]$, and six $[Au_4(SR)_2]$ rings fused or interlocked together. For other 93 thiolate-protected gold clusters, their structural decompositions based on the ring model are shown in Figures S9-S101.

2. Understanding the structural stabilities of thiolate-protected gold nanoclusters.

In Table 2, the average distance (d_1) between the gold atoms in the atomic structures at the center of ring and the gold atoms in the ring, and the average distance (d_2) between two adjacent gold atoms in each ring are given. The measured values of d_1 and d_2 for the $Au_4(SR)_4$, $Au_{10}(SR)_{10}$, and $Au_{12}(SR)_{12}$ complexes are also given in Table 2 for comparison. The very close d_1 and d_2 values of the rings and complexes suggest that the aurophilic interactions play an important role in stabilization of the thiolate-protected gold nanoclusters.[46,47] Specifically, the role of protection motifs $SR[Au(SR)]_x$ (x = 0, 1, 2, 3, ...) is not only for binding the surface gold atoms of the gold core via strong Au-S covalent bond, but also for generating the $[Au_m(SR)_n]$ rings with aurophilic interactions among the gold atoms within the rings. Considering the ring model and GUM altogether, the stabilities of thiolate-protected gold nanoclusters can be mainly attributed to the following four factors: (1) the high stabilities of the elementary blocks or secondary blocks for the formation of the gold cores, (2) the aurophilic interactions between two neighboring elementary blocks, (3) the strong Au-S covalent bonds, and (4) the aurophilic interactions among the protection motifs and gold cores.

Table 2. The average distance d_1 between the gold atoms in the atomic structures at the center of ring, and the average distance d_2 between two adjacent gold atoms in the ring of the thiolate-protected gold nanoclusters. The measured values of d_1 and d_2 for $Au_4(SR)_4$, $Au_{10}(SR)_{10}$, $Au_{12}(SR)_{12}$ complexes are also given for comparison.

Rings	d_1/Å	d_2/Å
$[Au_4(SR)_4]$	-	3.24
$[Au_4(SR)_n]$ (1 < n < 4)	-	3.23
$[Au_5(SR)_5]$	-	3.60
$[Au_5(SR)_n]$ (1 < n < 5)	-	3.47
$[Au_6(SR)_6]$	3.44	3.49
$[Au_6(SR)_n]$ (0 ≤ n ≤ 6)	3.20	3.56
$[Au_7(SR)_4]$ (n = 4 or 5)	3.07	3.57
$[Au_8(SR)_8]$	3.06	3.56
$[Au_8(SR)_n]$ (n = 4, 6, or 8)	3.27	3.32
$[Au_{10}(SR)_4]$	3.05	3.21
$[Au_{12}(SR)_4]$	3.00	3.02

3. Structural prediction.

Importantly, the ring model can be also used to predict new structures of the thiolate-protected gold clusters. To this end, a gold core should be constructed first. Based on the GUM,[14-16] the gold core of ligand-protected gold nanoclusters can be viewed as several elementary blocks (either the triangular Au_3 or tetrahedral Au_4, both satisfying the duet rule) fused or packed together. As an example, here, a new Au_{28} core composed of eight tetrahedral Au_4 units can be constructed (Figure 10). Next, based on the ring model, the protection motifs including four $SR[Au(SR)]_2$, six SR[Au(SR)], and two SR can be easily added to the Au_{28} core to yield a new $Au_{42}(SR)_{26}$ isomer, consisting of six $[Au_6(SR)_3]$ and one $[Au_{10}(SR)_4]$ rings (Figure S46). DFT computation shows that this new isomer has lower energy than two crystallized isomers reported previously,[44,48] thereby giving credence to the effectiveness of the ring model for predicting new and highly stable clusters.

Conclusion

In conclusion, a ring model is proposed to describe the interfacial interactions between $SR[Au(SR)]_x$ (x = 0, 1, 2, 3, ...) protection motifs and gold cores in thiolate-protected gold nanoclusters. A central concept of

the ring model is that the gold nanoclusters can be decomposed into several $[Au_m(SR)_n]$ (m = 4 - 8, 10, 12, and $0 \leq n \leq m$) rings, fused or interlocked together. The aurophilic interactions among these rings play an important role in stabilizing the thiolate-protected gold nanoclusters. The ring model not only provides a deep chemical insight into the interfacial interactions between protection motifs and gold core in thiolate-protected gold nanoclusters, but also offers a simple way to construct and design new nanoclusters for future confirmation by experiments.

Declarations

Conflicts of interest

The authors declare no conflicts of interest.

Acknowledgment

WWX is supported by Natural Science Foundation of China (Grant No. 11974195) and the Natural Science Foundation of Ningbo (Grant No. 2019A610182). WWX also acknowledges computational support from National Supercomputing Center in Guangzhou (NSCC-GZ).

References

1. Häkkinen, H. The gold-sulfur interface at the nanoscale. *Nat. Chem.* **4**, 443–455 (2012).
2. Jadzinsky, P. D., Calero, G., Ackerson, C. J., Bushnell, D. A. & Kornberg, R. D. Structure of a thiol monolayer-protected gold nanoparticle at 1.1 Å resolution. *Science* **318**, 430–433 (2007).
3. Pei, Y. & Zeng, X. C. Investigating the structural evolution of thiolate protected gold clusters from first-principles, *Nanoscale* **4**, 4054–4072 (2012).
4. Jin, R., Zeng, C., Zhou, M. & Chen, Y. Atomically precise colloidal metal nanoclusters and nanoparticles: Fundamentals and opportunities. *Chem. Rev.* **116**, 10346–10413 (2016).
5. Ma, Z., Wang, Pu., Xiong, L. & Pei, Y. Thiolate-protected gold nanoclusters: Structural prediction and the understandings of electronic stability from first principles simulations. *WIREs: Comput. Mol. Sci.* **7**, e1315 (2017).
6. Jin, R., Pei, Y. & Tsukuda, T. Controlling nanoparticles with atomic precision. *Acc. Chem. Res.* **52**, 1 (2019).
7. Pei, Y., Wang, P., Ma, Z. & Xiong, L. Growth-rule-guided structural exploration of thiolate-protected gold nanoclusters. *Acc. Chem. Res.* **52**, 23–33 (2019).
8. Häkkinen, H., Walter, M. & Gronbeck, H. Divide and protect: Capping gold nanoclusters with molecular gold-thiolate rings. *J. Phys. Chem. B* **110**, 9927–9931 (1996).
9. Walter, M., Akola, J., Lopez-Acevedo, O., Jadzinsky, P. D., Calero, G., Ackerson, C. J., Whetten, R. L., Gronbeck, H. & Häkkinen, H. A unified view of ligand-protected gold clusters as superatom

complexes. *Proc. Natl. Acad. Sci.* **105**, 9157–9162 (2008).

10. Cheng, L., Ren, C., Zhang, X. & Yang, J. New insight into the electronic shell of $Au_{38}(SR)_{24}$: A superatomic molecule. *Nanoscale* **5**, 1475–1478 (2013).
11. Cheng, L., Yuan, Y., Zhang, X. & Yang, J. Superatom networks in thiolate-protected gold nanoparticles. *Angew. Chem. Int. Ed.* **52**, 9035 – 9039 (2013).
12. Zubarev, D. Y. & Boldyrev, A. I. Developing paradigms of chemical bonding: Adaptive natural density partitioning. *Phys. Chem. Chem. Phys.* **10**, 5207–5217 (2008).
13. Natarajan, G., Mathew, A., Negishi, Y., Whetten, R. L. & Pradeep, T. A unified framework for understanding the structure and modifications of atomically precise monolayer protected gold clusters. *J. Phys. Chem. C* **119**, 27768–27785 (2015).
14. Xu, W. W., Zhu, B., Zeng, X. C. & Gao, Y. A grand unified model for liganded gold clusters. *Nat. Commun.* **7**, 13574 (2016).
15. Xu, W. W., Zeng, X. C. & Gao, Y. $Au_{13}(8e)$: A secondary block for describing a special group of liganded gold clusters containing icosahedral Au_{13} motifs. *Chem. Phys. Lett.* **675**, 35–39 (2017).
16. Xu, W. W., Zeng, X. C. & Gao, Y. Application of electronic counting rules for ligand-protected gold nanoclusters. *Acc. Chem. Res.* **51**, 2739–2747 (2018).
17. Taylor, M. & Mpourmpakis, G. Thermodynamic stability of ligand-protected metal nanoclusters. *Nat. Commun.* **8**, 15988 (2017).
18. Zhu, M., Aikens, C. M., Hollander, F. J., Schatz, G. C. & Jin, R. Correlating the crystal structure of a thiol-protected Au_{25} cluster and optical properties. *J. Am. Chem. Soc.* **130**, 5883–5885 (2008).
19. Heaven, M. W., Dass, A., White, P. S., Holt, K. M. & Murray, R. W. Crystal structure of the gold nanoparticle $[N(C_8H_{17})_4][Au_{25}(SCH_2CH_2Ph)_{18}]$. *J. Am. Chem. Soc.* **130**, 3754–3755 (2008).
20. Akola, J., Walter, M., Whetten, R. L., Häkkinen, H. & Grönbeck, H. On the structure of thiolate-protected Au_{25}. *J. Am. Chem. Soc.* **130**, 3756–3757 (2008).
21. Liu, C., Li, T., Li, G., Nobusada, K., Zeng, C., Pang, G., Rosi, N. L. & Jin, R. Observation of body-centered cubic gold nanocluster. *Angew. Chem. Int. Ed.* **54**, 9826–9829 (2015).
22. Bonasia, P. J., Gindelberger, D. E. & Arnold, J. Synthesis and characterization of gold(I) thiolates, selenolates, and tellurolates: X-ray crystal structures of $Au_4[TeC(SiMe_3)_3]_4$, $Au_4[SC(SiMe_3)_3]_4$, and $Ph_3PAu[TeC(SiMe_3)_3]$. *Inorg. Chem.* **32**, 5126–5131 (1993).
23. Xu, G. T., Wu, L. L., Chang, X. Y., Ang, T. W. H., Wong, W. Y., Huang, J. S. & Che, C. M. Solvent-induced cluster-to-cluster transformation of homoleptic gold(i) thiolates between catenane and ring-in-ring structures. *Angew. Chem. Int. Ed.* **58**, 2–12 (2019).
24. Xiong, L., Yang, S., Sun, X., Chai, J., Rao, B., Yi, L., Zhu, M. & Pei Y. Structure and electronic structure evolution of thiolate-protected gold nanoclusters containing quasi face-centered-cubic kernels. *J. Phys. Chem. C* **122**, 14898–14907 (2018).

25. Zeng, C., Liu, C., Chen, Y., Rosi, N. L. & Jin, R. Gold-thiolate ring as a protecting motif in the $Au_{20}(SR)_{16}$ nanocluster and implications. *J. Am. Chem. Soc.* **136**, 11922–11925 (2014).
26. Yang, S., Chen, S., Xiong, L., Liu, C., Yu, H., Wang, S., Rosi, N. L., Pei, Y. & Zhu, M. Total structure determination of Au_{16}(S-Adm)$_{12}$ and Cd_1Au_{14}(S*t*Bu)$_{12}$ and implications for the structure of $Au_{15}(SR)_{13}$. *J. Am. Chem. Soc.* **140**, 10988–10994 (2018).
27. Dass, A., Jones, T., Rambukwella, M., Crasto, D., Gagnon, K. J., Sementa, L., De Vetta, M., Baseggio, O., Aprà, E., Stener, M. & Fortunelli, A. Crystal structure and theoretical analysis of green gold Au_{30}(S–tBu)$_{18}$ nanomolecules and their relation to $Au_{30}S$(S–tBu)$_{18}$. *J. Phys. Chem. C* **120**, 6256–6261 (2016).
28. Dong, H., Liao, L. & Wu, Z. Two-way transformation between fcc- and nonfcc-structured gold nanoclusters. *J. Phys. Chem. Lett.* **8**, 5338–5343 (2017).
29. Pei, Y., Pal, R., Liu, C., Gao, Y., Zhang, Z. & Zeng, X. C. Interlocked catenane-like structure predicted in $Au_{24}(SR)_{20}$: Implication to structural evolution of thiolated gold clusters from homoleptic gold(i) thiolates to core-stacked nanoparticles. *J. Am. Chem. Soc.* **134**, 3015–3024 (2012).
30. Wiseman, M. R., Marsh, P. A., Bishop, P. T., Brisdon, B. J. & Mahon, M. F. Homoleptic Gold Thiolate Catenanes. *J. Am. Chem. Soc.* **122**, 12598–12599 (2000).
31. Pei, Y., Tang, J., Tang, X., Huang, Y. & Zeng, X. C. New structure model of $Au_{22}(SR)_{18}$: Bitetrahederon golden kernel enclosed by [$Au_6(SR)_6$] Au(I) complex. *J. Phys. Chem. Lett.* **6**, 1390–1395 (2015).
32. Chen, S., Xiong, L., Wang, S., Ma, Z., Jin, S., Sheng, H., Pei, Y. & Zhu, M. Total structure determination of Au_{21}(S-Adm)$_{15}$ and geometrical/electronic structure evolution of thiolated gold nanoclusters. *J. Am. Chem. Soc.* **138**, 10754–10757 (2016).
33. Zeng, C., Li, T., Das, A., Rosi, N. L. & Jin, R. Chiral structure of thiolate-protected 28-gold-atom nanocluster determined by X-ray crystallography. *J. Am. Chem. Soc.* **135**, 10011–10013 (2013).
34. Das, A., Li, T., Nobusada, K., Zeng, C., Rosi, N. L. & Jin, R. Nonsuperatomic $[Au_{23}(SC_6H_{11})_{16}]^-$ nanocluster featuring bipyramidal Au_{15} kernel and trimeric $Au_3(SR)_4$ motif. *J. Am. Chem. Soc.* **135**, 18264–18267 (2013).
35. Zeng, C., Qian, H., Li, T., Li, G., Rosi, N. L., Yoon, B., Barnett, R. N., Whetten, R. L., Landman, U. & Jin, R. Total structure and electronic properties of the gold nanocrystal $Au_{36}(SR)_{24}$. *Angew. Chem. Int. Ed.* **51**, 13114–13118 (2012).
36. Wang, P., Sun, X., Liu, X., Xiong, L., Ma, Z. & Pei. Y. Theoretical predictions of a new ~14 kDa core-mass thiolate-protected gold nanoparticle: $Au_{68}(SR)_{36}$. *J. Phys. Chem. Lett.* **8**, 1248–1252 (2017).
37. Dong, H., Liao, L., Zhuang, S., Yao, C., Chen, J., Tian, S., Zhu, M., Liu, X., Li, L. & Wu, Z. A novel double-helical-kernel evolution pattern of gold nanoclusters: alternate single-stranded growth at both ends. *Nanoscale* <background-color:#FFCC66;bu>9</background-color:#FFCC66;bu>, 3742–3746 (2017).
38. Zeng, C., Liu, C., Chen, Y., Rosi, N. L. & Jin, R. Atomic structure of self-assembled monolayer of thiolates on a tetragonal Au_{92} nanocrystal. *J. Am. Chem. Soc.* **138**, 8710–8713 (2016).

39. Zeng, C., Chen, Y., Liu, C., Nobusada, K., Rosi, N. L. & Jin, R. Gold tetrahedra coil up: Kekulé-like and double helical superstructures. *Sci. Adv.* **1**, e1500425 (2015).
40. Tian, S., Li, Y., Li, M., Yuan, J., Yang, J., Wu, Z. & Jin, R. Structural isomerism in gold nanoparticles revealed by X-ray crystallography. *Nat. Commun.* **6**, 8667, (2015).
41. Chen, Y., Liu, C., Tang, Q., Zeng, C., Higaki, T., Das, A., Jiang, D., Rosi, N. L. & Jin, R. Isomerism in $Au_{28}(SR)_{20}$ nanocluster and stable structures. *J. Am. Chem. Soc.* **138**, 1482–1485 (2016).
42. Yang, L., Wang, P., Yang, Z. & Pei, Y. Effect of thiolate-ligand passivation on the electronic structure and optical absorption properties of ultrathin one and two-dimensional gold nanocrystals. *Nanoscale* **12**, 5554–5566 (2020).
43. Zheng, M. & Xu, W. W. Structural transformations from thiolate-protected gold nanoclusters to Au(I)-S complexes by introducing three-coordinated μ_3-sulfido and four-coordinated μ_4-sulfido motifs. *J. Phys. Chem. C* https://doi.org/10.1021/acs.jpcc.0c03971 (2020).
44. Zhuang, S., Liao, L., Zhao, Y., Yuan, J., Yao, C., Liu, X. Li, J. Deng, H., Yang J. & Wu, Z. Is the kernel–staples match a key–lock match? *Chem. Sci.* **9**, 2437–2442 (2018).
45. Das, A., Li, T., Li, G., Nobusada, K., Zeng, C., Rosi, N. L. & Jin, R. Crystal structure and electronic properties of a thiolate-protected Au_{24} nanocluster. *Nanoscale* **6**, 6458–6462 (2014).
46. Schmidbaur, H. & Schier, A. Aurophilic interactions as a subject of current research: An up-date. *Chem. Soc. Rev.* **41**, 370–412 (2012).
47. Yam, V. W., Au, V. K. & Leung, S. Y. Light-emitting self-assembled materials based on d^8 and d^{10} transition metal complexes. *Chem. Rev.* **115**, 7589–7728 (2015).
48. Zhuang, S., Liao, L., Yuan, J., Xia, N., Zhao, Y., Wang, C., Gan, Z., Yan, N., He, L., Li, J., Deng, H., Guan, Z., Yang, J., Wu, Z. Fcc versus non-fcc structural isomerism of gold nanoparticles with kernel atom packing dependent photoluminescence. *Angew. Chem. Int. Ed.* **58**, 4510–4514 (2019).

Figures

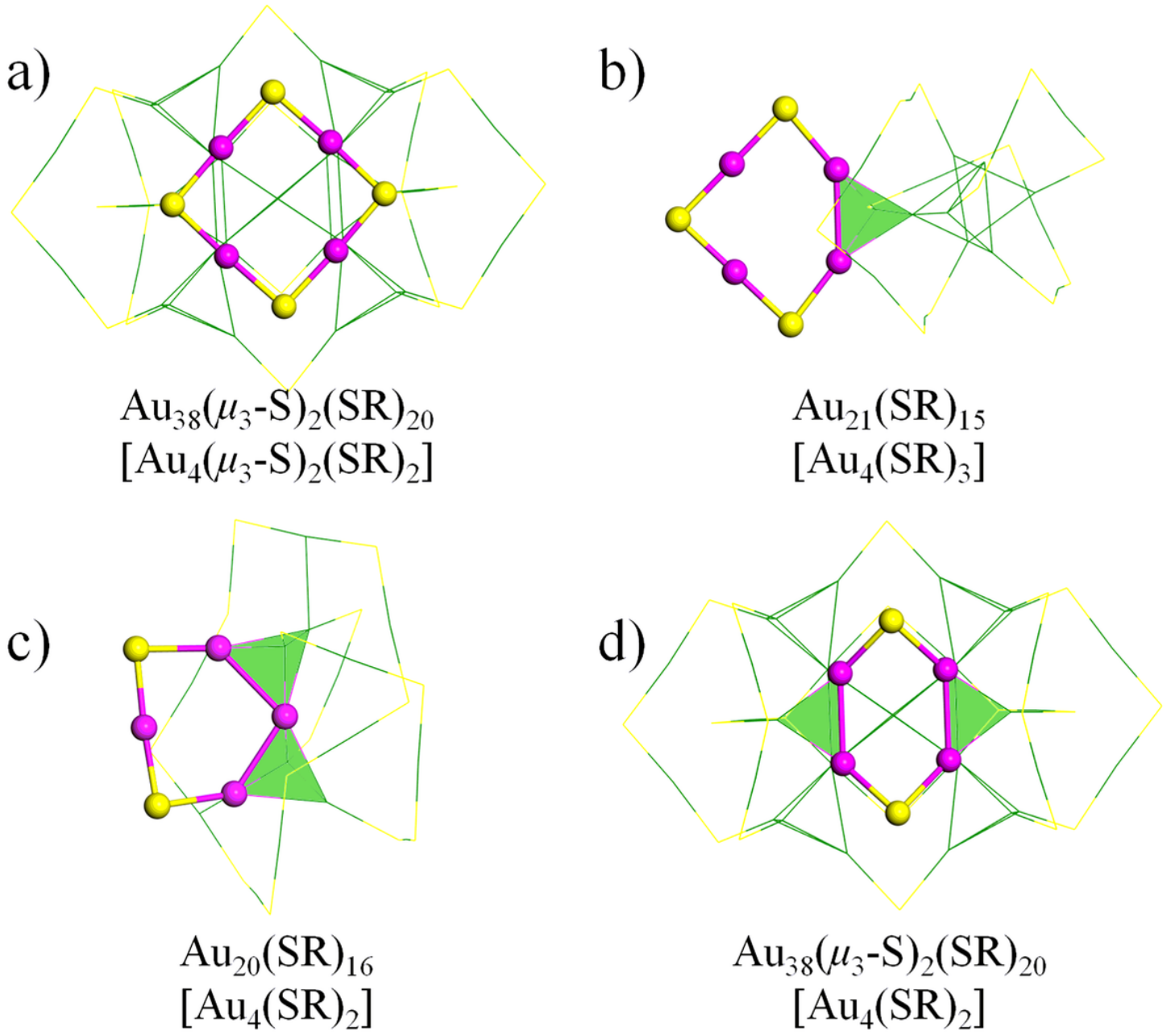

Figure 1

The [Au4(μ3-S)2(SR)2] ring in Au38(μ3-S)2(SR)20 (a), [Au4(SR)3] ring in Au21(SR)15 (b), and two [Au4(SR)2] rings in Au20(SR)16 (c) and Au38(μ3-S)2(SR)20 (d). The Au atoms in wine and S atoms in yellow in [Au4(μ3-S)2(SR)2], [Au4(SR)3], and [Au4(SR)2] rings are represented by solid balls, and the other atoms are denoted by lines. The tetrahedral Au4 and triangular Au3 elementary blocks that are connected with the rings are filled with green color. Au: wine and dark green; S: yellow. The R groups are omitted for clarity.

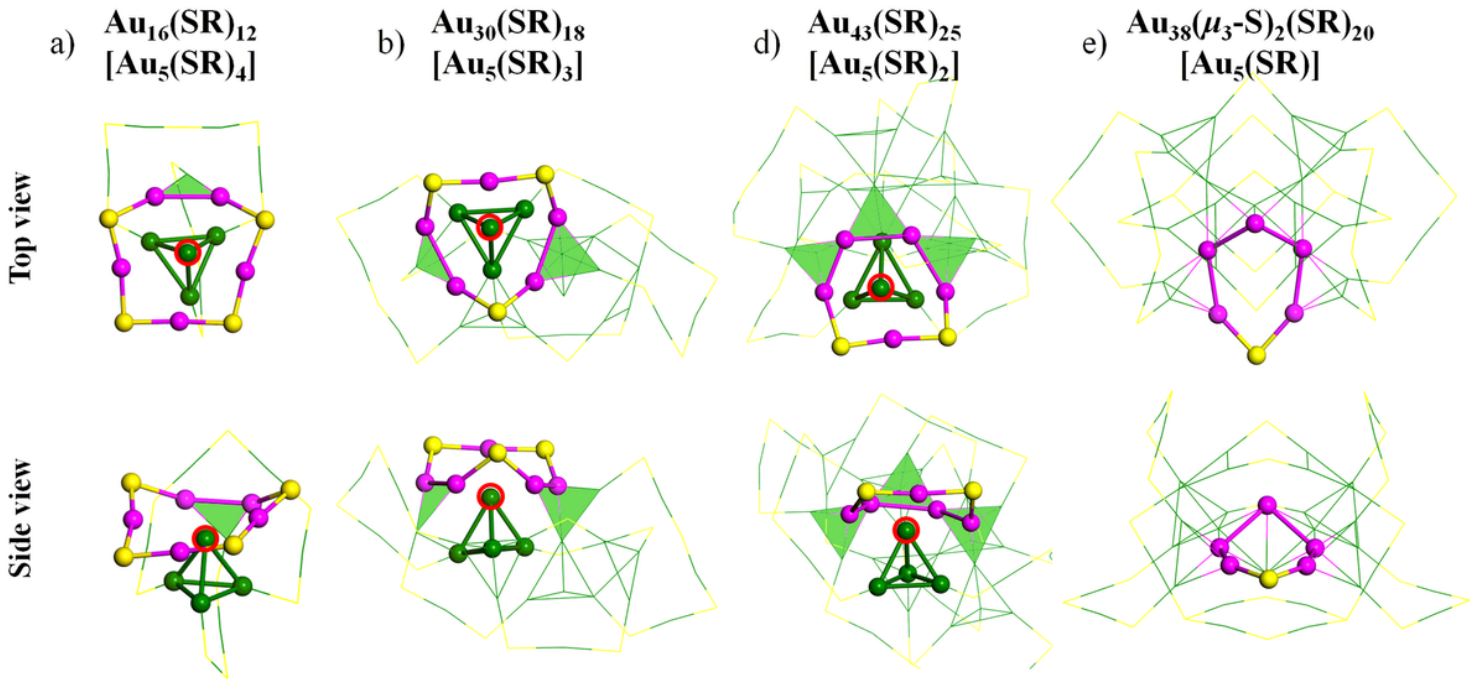

Figure 2

The top (upper panels) and side (lower panels) of [Au5(SR)4] ring in Au16(SR)12 (a), [Au5(SR)3] rings in Au30(SR)18 (b), [Au5(SR)2] ring in Au43(SR)25 (c), and [Au5(SR)] ring in Au38(μ3-S)2(SR)20 (d). The Au atoms in wine and S atoms in yellow in [Au5(SR)4], [Au5(SR)3], [Au5(SR)2] and [Au5(SR)] rings and Au atoms in green in tetrahedral Au4 structures beneath the [Au5(SR)4], [Au5(SR)3], and [Au5(SR)2] rings are represented by solid balls, and the other atoms are denoted by lines. The tetrahedral Au4 and triangular Au3 elementary blocks that are connected with the rings are filled with green color. A special gold atom near the [Au5(SR)n] ring without binding with the SR motif is highlighted by a red circle. Au: wine and dark green; S: yellow. The R groups are omitted for clarity.

Figure 3

The [Au6(SR)6] ring in Au22(SR)18 (a), [Au6(SR)5] ring in Au21(SR)15 (b), [Au6(SR)4] rings in Au28(SR)20 (c) and Au23(SR)16- (d), [Au6(SR)3] rings in Au30(SR)18 (e) and Au36(SR)24 (f), Au68(SR)36 (g), [Au6(SR)2] rings in Au34(SR)22 (h) and Au92(SR)44 (i), [Au6(SR)] ring in Au92(SR)44 (j), and [Au6] ring in Au40(SR)24 (k). The Au atoms in wine and S atoms in yellow in [Au6(SR)n] ($0 \leq n \leq 6$) rings are represented by solid balls, and the other atoms are denoted by lines. The tetrahedral Au4 and triangular Au3 elementary blocks that are connected with the rings are filled with green color. Au: wine and dark green; S: yellow. The R groups are omitted for clarity.

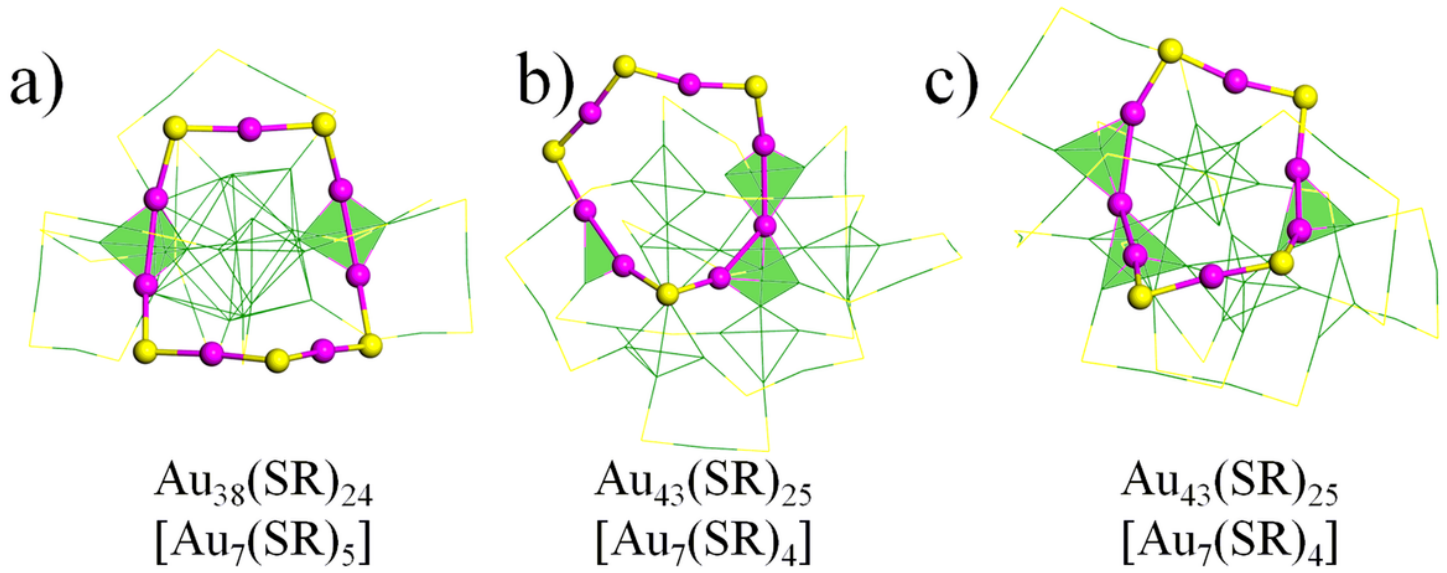

Figure 4

The [Au7(SR)5] ring in Au38(SR)24 (a) and two types of [Au7(SR)4] rings in Au43(SR)25 (b and c). The Au atoms in wine and S atoms in yellow in rings are represented by solid balls, and the other atoms are denoted by lines. The tetrahedral Au4 and triangular Au3 elementary blocks that are connected with the rings are filled with green color. Au: wine and dark green; S: yellow. The R groups are omitted for clarity.

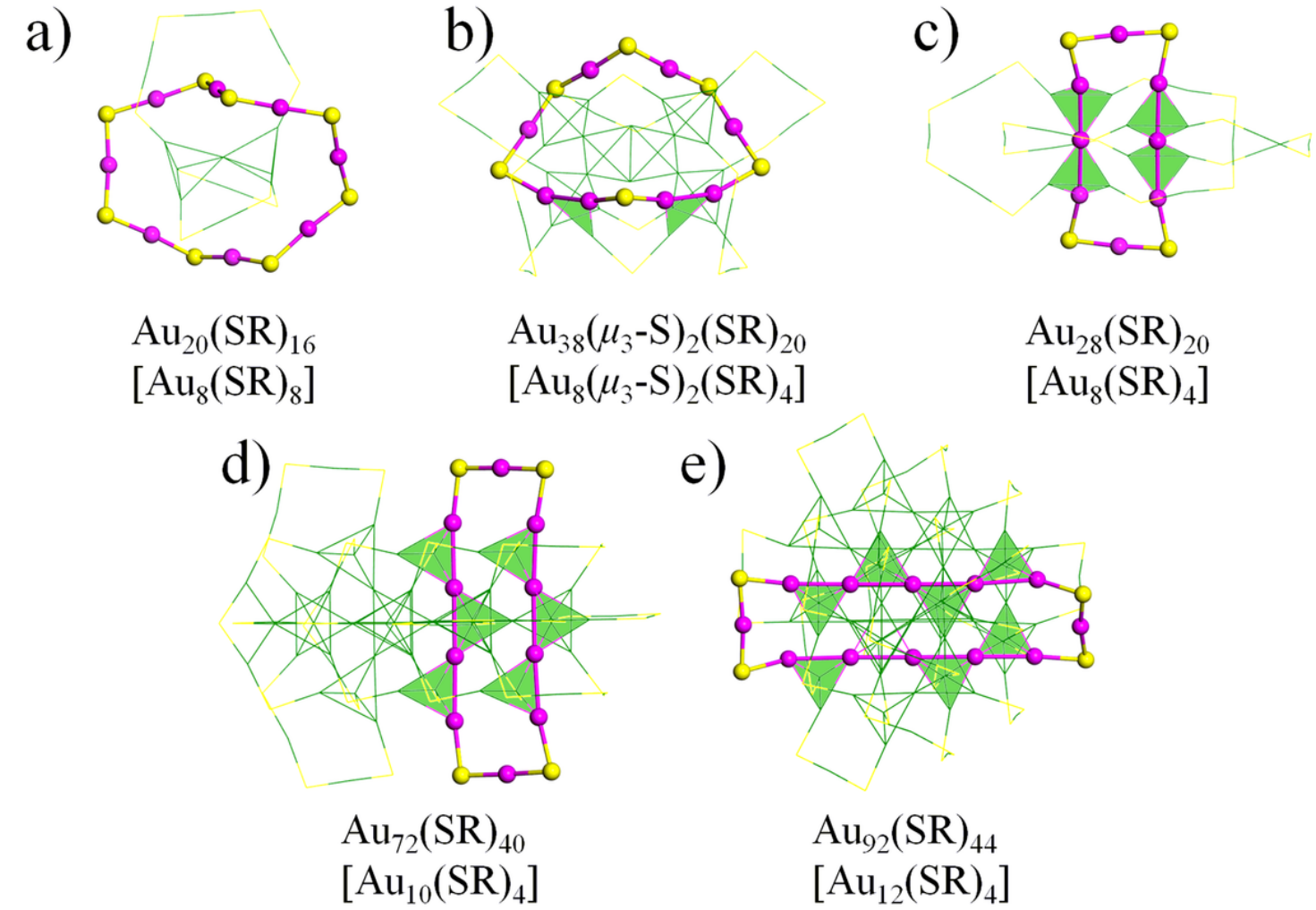

Figure 5

The [Au8(SR)8] ring in Au20(SR)16 (a), [Au8(μ3-S)2(SR)4] ring in Au38(μ3-S)2(SR)20 (b), [Au8(SR)4] ring in Au28(SR)20 (c), [Au10(SR)4] ring in Au72(SR)40 (d), and [Au12(SR)4] ring in Au92(SR)44 (e). The Au atoms in wine and S atoms in yellow in rings are represented by solid balls, and the other atoms are denoted by lines. The tetrahedral Au4 and triangular Au3 elementary blocks that are connected with the rings are filled with green color. Au: wine and dark green; S: yellow. The R groups are omitted for clarity.

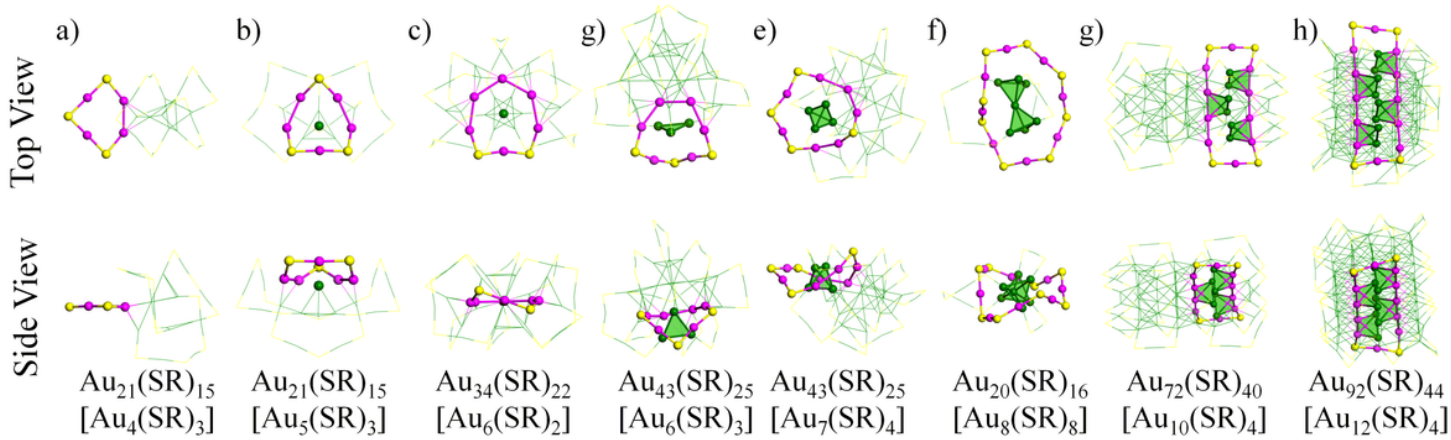

Figure 6

Top (upper panels) and side (lower panels) views of the atomic structures (solid balls in dark blue) at the center of rings, in which the Au atoms in wine and S atoms in yellow are represented by solid balls. Au: wine and dark green; S: yellow. The R groups are omitted for clarity.

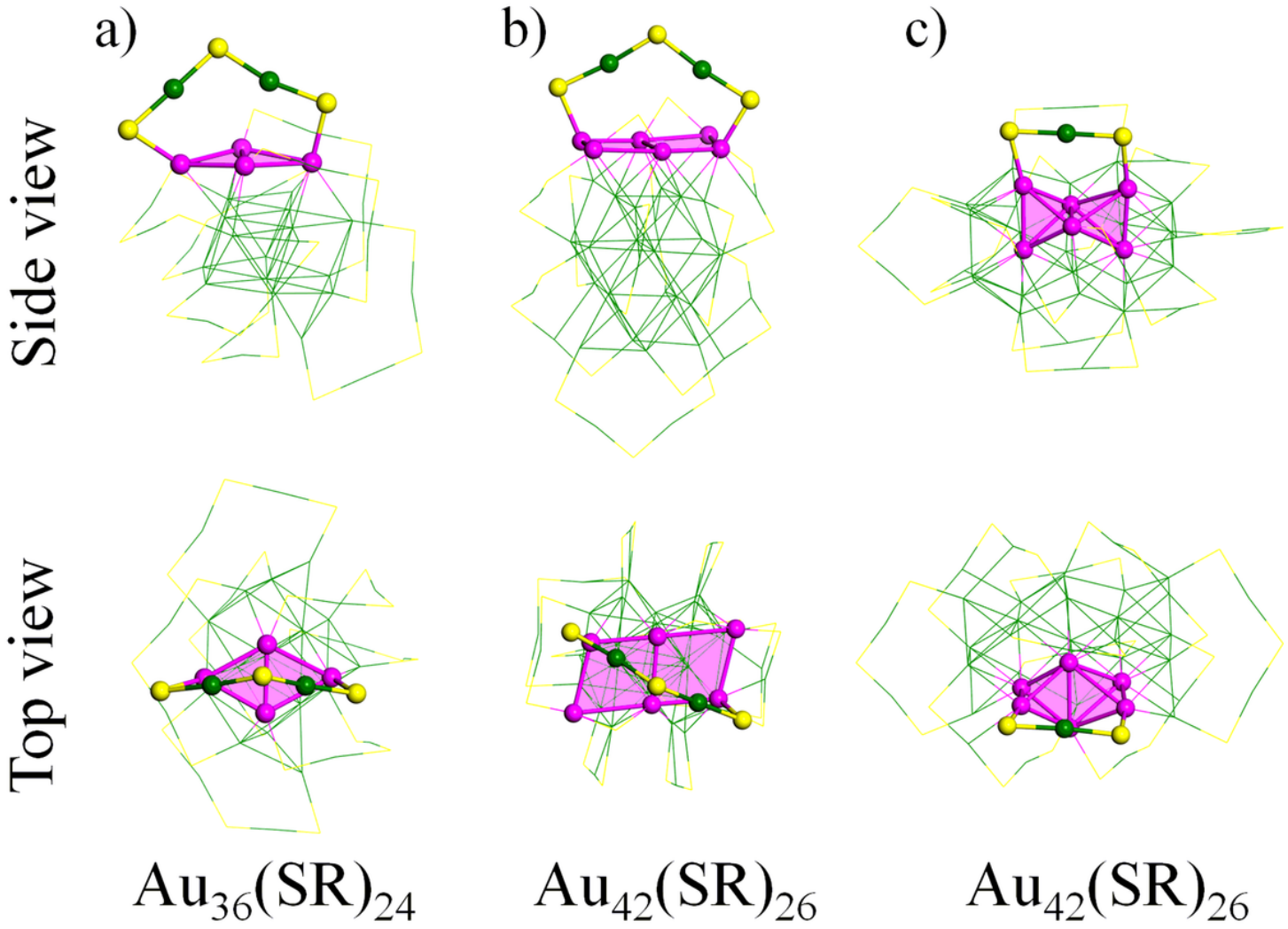

Figure 7

Top (upper panels) and side (lower panels) views of SR[Au(SR)]2 motif binding with the Au(111) facet (solid balls in wine) in Au36(SR)24 (a), SR[Au(SR)]2 motif binding with the Au(100) facet (solid balls in wine) in Au42(SR)26 (b), and SR[Au(SR)] motif binding with the Au6 structure (solid balls in wine) formed by two fused tetrahedrons Au4 via sharing one Au-Au edge in Au42(SR)26 (c). Au: wine and dark green; S: yellow. The R groups are omitted for clarity.

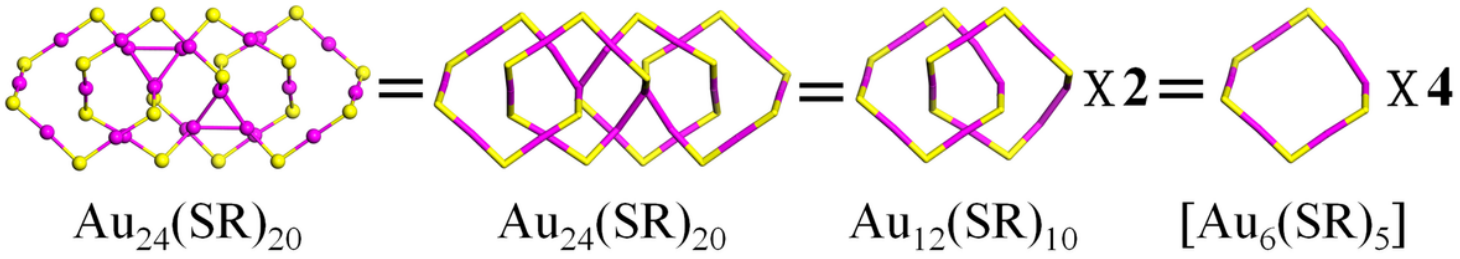

Figure 8

The structural decompositions of Au24(SR)20 into four [Au6(SR)5] rings. Au: wine; S: yellow. The R groups are omitted for clarity.

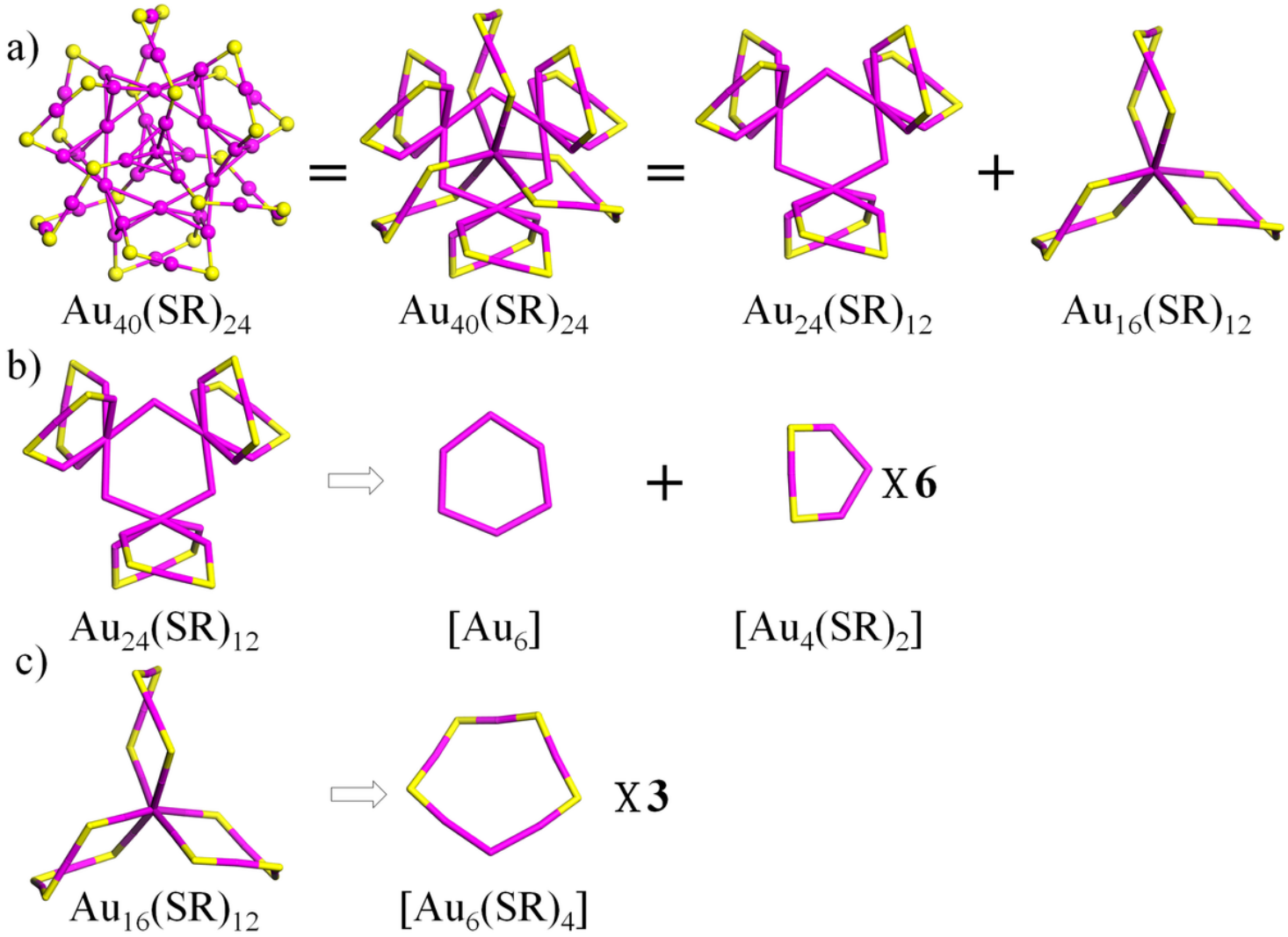

Figure 9

The structural decompositions of Au40(SR)24 into six [Au4(SR)2], one [Au6], and four [Au6(SR)5] rings. Au: wine; S: yellow. The R groups are omitted for clarity.

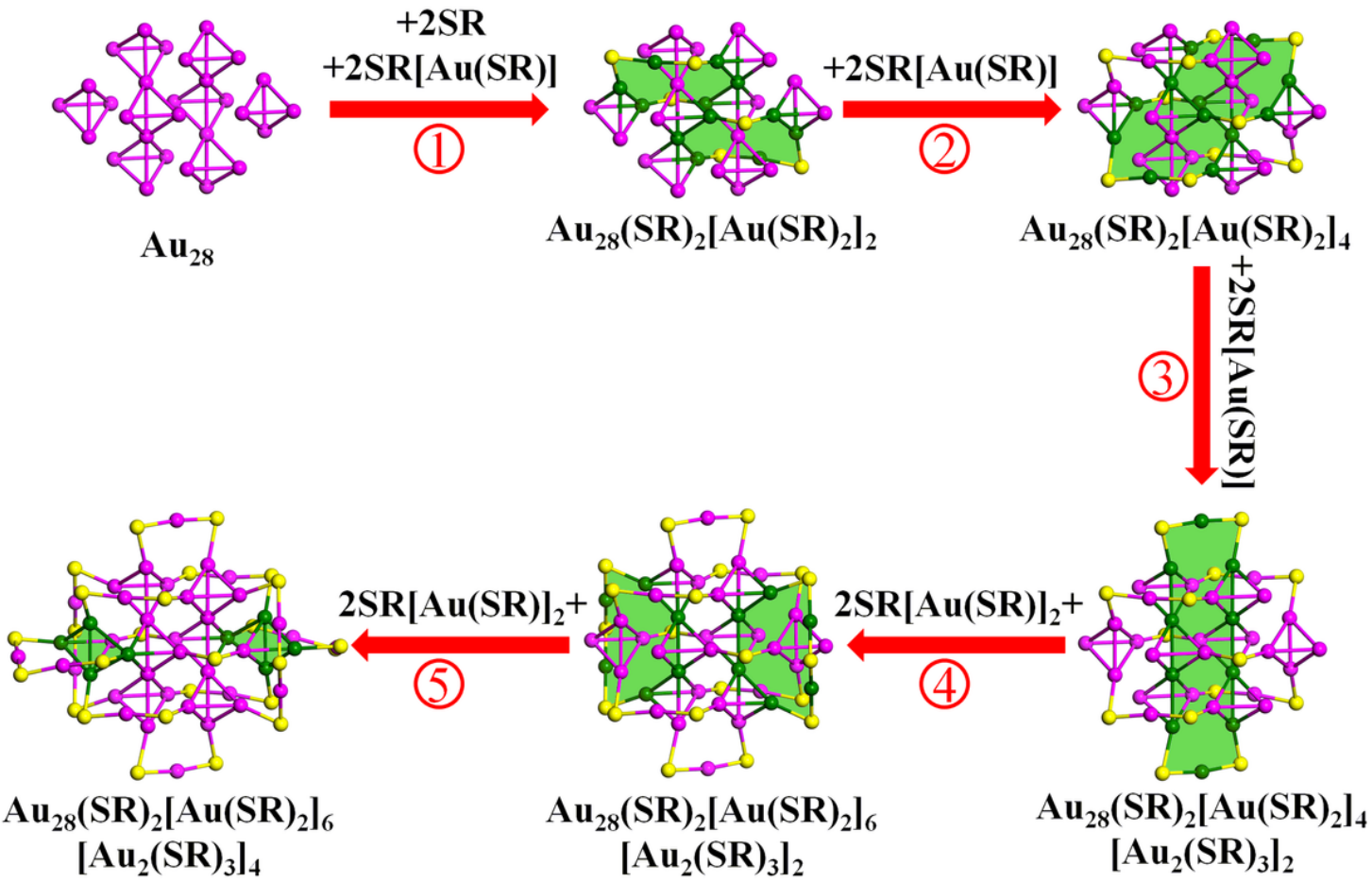

Figure 10

The structural prediction of a new Au42(SR)26 isomer based on the ring model and GUM. The rings and Au(111) facets are filled with green color. Au: wine and dark green; S: yellow. The R groups are omitted for clarity.

Supplementary Files

This is a list of supplementary files associated with this preprint. Click to download.

- ligandcoreSI.docx